

Nicotinic receptors modulate ongoing synchronous spontaneous activity of prefrontal cortex: Consequences for conscious processing

Fani Koukoulis^{a,b,1}, Marie Rooy^c, Jean-Pierre Changeux^{b,1}, and Uwe Maskos^{a,b,1}

^aNeurobiologie Intégrative des Systèmes Cholinergiques, Institut Pasteur, Paris F-75724 cedex 15, France; ^bCNRS UMR 3571, Institut Pasteur, Paris F-75724 cedex 15, France; and ^cGroup for Neural Theory, Laboratoire de Neurosciences Cognitives, INSERM Unité 969, Département d'Études Cognitive, École Normale Supérieure, Paris, France

Contributed by Jean-Pierre Changeux, August 31, 2016 (sent for review June 25, 2016; reviewed by Rafael Malach and Marina R. Picciotto)

The prefrontal cortex (PFC) plays an important role in cognitive processes, including access to consciousness. The PFC receives significant cholinergic innervation and nicotinic acetylcholine receptors (nAChRs) contribute greatly to the effects of acetylcholine signaling. Using *in vivo* two-photon imaging of both awake and anesthetized mice, we recorded spontaneous, ongoing neuron activity in layer II/III in the PFC of WT mice and mice deleted for different nAChR subunits. As in humans, this activity is characterized by synchronous ultraslow fluctuations and neuronal synchronicity is disrupted by light general anesthesia. Both the $\alpha 7$ and $\beta 2$ nAChR subunits play an important role in the generation of ultraslow fluctuations that occur to a different extent during quiet wakefulness and light general anesthesia. The $\beta 2$ subunit is specifically required for synchronized activity patterns. Furthermore, chronic application of mecamylamine, an antagonist of nAChRs, disrupts the generation of ultraslow fluctuations. Our findings provide new insight into the ongoing spontaneous activity in the awake and anesthetized state, and the role of cholinergic neurotransmission in the orchestration of cognitive functions.

nicotinic receptor | consciousness | ultraslow fluctuations | anesthesia | prefrontal cortex

The prefrontal cortex (PFC) plays an important role in cognitive processes such as attention (1), working memory (2), decision making (3), social behavior (4), and emotions (5). Current theories consider the PFC a key player in conscious processing (6–8). Deficits in prefrontal function, including attention, are noted in several neuropsychiatric disorders, including schizophrenia, attention deficit/hyperactivity syndrome, addiction, depression, and autism (9).

In humans, as in rodent models, cholinergic innervation of the PFC regulates cognitive processes and neuronal activity. For example, in rodents, removing PFC cholinergic innervation reduces attention performance, whereas stimulation of cholinergic projections causes enhancement (10). Many studies in both animal models and humans have shown that nicotinic acetylcholine receptors (nAChRs) are of particular importance for cognitive functions, reward, aging, and for pathologies like Alzheimer's Disease (11). For example, deletion of the $\alpha 7$ and $\beta 2$ nAChR subunits in mice impairs behaviors, such as exploration and attention (12–16). Importantly, lesions of the prefrontal cortex (PrLC) in WT mice cause deficits in social behavior, similar to those observed in $\beta 2$ KO mice, whereas re-expression of the $\beta 2$ subunit in the PrLC of $\beta 2$ KO mice rescues their social interaction (4). Similarly, re-expression of $\beta 2$ subunits in the PrLC of $\beta 2$ KO mice fully restored their attentional performance in the five-choice serial reaction time task (16).

Ongoing spontaneous activity is known to occur in developing and adult brain and its physiological importance has been emphasized (17). Recordings in humans indicate that ongoing activity constantly fluctuates in a tightly correlated manner across distant brain regions, forming reproducible patterns with rich temporal dynamics and spatial organization (18). The potential contribution of spontaneous activity to conscious processing has been suggested and simulations helped characterize two main modes of activity:

an active mode characterized by rapid and sustained activity (“ignition”) (19), which contributes to the signature of “conscious access,” and a resting mode with spontaneous ultraslow (<0.1 Hz) fluctuations (USFs) of low amplitude (18). It has been suggested that ignition and ultraslow spontaneous fluctuations share similar mechanisms (18). Independently, electrophysiological recordings in animal models have distinguished “up” and “down” states (20), and the possibility is considered here that up states coincide with USFs in humans. Furthermore, *in vivo* recordings in animal models (21) reveal that, similar to humans, USFs persist under general anesthesia, yet with a lower amplitude (22, 23). Under anesthesia, the dominating functional configurations have low information capacity and lack negative correlations (24). Conversely, in the awake state a dynamic exploration of a rich, flexible repertoire of functional configurations takes place, including ignition, in the course of conscious access. However, to our knowledge, the pharmacology and biochemistry of these processes remain unexplored.

To address this gap in our knowledge, using *in vivo* Ca^{2+} imaging we recorded and compared the spontaneous activity patterns in the PrLC of both awake mice and mice under general anesthesia, a condition where conscious processing is known to be altered (25). These recordings point to spontaneous and infrequent coherent states with high firing rates, analogous to USFs. Our findings reveal a distinct role of nAChRs in the ongoing synchronous neuronal activity of the PFC in awake and anesthetized animals, shedding light on a possible involvement of nAChRs in conscious processing.

Significance

The human brain exhibits ongoing spontaneous activity characterized by very slow frequency fluctuations. These synchronously firing populations are considered to play a key role in conscious processes. We identified ultraslow fluctuations (USFs) in awake and anesthetized mice using two-photon imaging in the prefrontal cortex, a brain region involved in higher cognitive processes. Using transgenic mice, we demonstrate a crucial role for nicotinic acetylcholine receptors (nAChRs) in the generation of ultraslow fluctuations and their synchronicity, processes that are affected by deletion of nAChR subunits and general anesthetics like isoflurane. This work allows further dissection of the underlying mechanisms, and predicts that in humans with nAChR polymorphisms or copy number variation these processes might be altered, resulting in neuropsychiatric disorders.

Author contributions: F.K., J.-P.C., and U.M. designed research; F.K. performed research; F.K. and M.R. analyzed data; and F.K., J.-P.C., and U.M. wrote the paper.

Reviewers: R.M., Weizmann Institute of Science; and M.R.P., Yale University School of Medicine.

The authors declare no conflict of interest.

¹To whom correspondence may be addressed. Email: fani.koukoulis@pasteur.fr, changeux@pasteur.fr, or umaskos@pasteur.fr.

This article contains supporting information online at www.pnas.org/lookup/suppl/doi:10.1073/pnas.1614417113/-/DCSupplemental.

Results

USFs Contribute to Mouse PFC Spontaneous Activity. The recognition of the “default mode” network (26) started a long-lasting interest in the significance of the human brain’s ongoing or intrinsic activity, which is characterized by synchronous USFs of activity, often taking seconds to develop (18). USFs have been recorded in the cortex of awake humans and primates, and also under anesthesia (27–30). The neuronal mechanisms that generate spontaneous resting-state fluctuations, together with the ignition dynamics, are unknown and remain a matter of debate.

To explore these issues *in vivo*, we used the mouse as a model together with two-photon imaging of spontaneous neuronal activity patterns recorded through a chronic cranial window in layer II/III of the PrLC (Fig. S1 A and B). Neurons of the PrLC were transduced with an adeno-associated viral vector (AAV) expressing the fluorescent calcium indicator GCaMP6f (Materials and Methods and SI Materials and Methods). Four weeks after AAV injection, the majority of layer II/III neurons exhibited green fluorescence (Figs. S1 C–E). We first studied the activity patterns of 3-mo-old awake head-fixed WT mice, where we simultaneously monitored the spontaneously occurring somatic GCaMP6f Ca^{2+} transients in multiple individual cells, and estimated the neural spiking rates through deconvolution of calcium transients (SI Materials and Methods). The mice were awake and reactive, as monitored by an infrared camera. A typical example of neural population activity is shown in Fig. 1A. To identify patterns of activity and USFs in populations of simultaneously recorded neurons, we studied the distribution of their time varying mean activity (see Materials and Methods and SI Materials and Methods for details). In Fig. 1, the USFs correspond to population activities in red and basal activities correspond to population activities in blue (Figs. 1 B and C). Interestingly, awake WT mice exhibited USFs with a frequency similar to that observed in humans (below 0.1 Hz) (17, 31). These frequencies are slower than those observed in the cardiac (0.6–1.2 Hz) and respiratory cycles (0.1–0.5 Hz) (31). The activity patterns were then analyzed to detect synchronous activity in populations of simultaneously imaged neurons, as previously described (20) (Materials and Methods). The number of simultaneously imaged cells ranged from 4 to 71 neurons, with a mean value of 36 neurons ($n = 2,900$ cells in 11 mice). In the awake state, we detected robust synchronicity in the neuronal populations (Fig. 1 D1). Our recordings indicate that, similar to awake humans, the ongoing activity in a mouse brain constantly fluctuates and exhibits synchronously firing neuronal activity, making the mouse a reliable model for studying some of the elementary physiological processes associated with conscious processing in humans.

USFs Persist Under Light General Anesthesia, but Synchronicity Is Disrupted. General anesthesia differentially alters states of consciousness and access to conscious content (8). The ability of general anesthesia to induce safe and reversible loss of consciousness poses the most complex question of how a simple chemical can affect conscious experience (32). General anesthetics may directly or indirectly affect conscious processing by the cerebral cortex (33); however, the neurobiological mechanisms involved in this interaction are largely unknown. We thus performed Ca^{2+} imaging of mainly pyramidal cells in the PrLC of lightly anesthetized WT mice (0.8% isoflurane), and compared their activity patterns with those recorded in awake mice (Fig. 1 A2–D2). Interestingly, the USFs persist under light general anesthesia, with no significant difference between the populations that exhibit USFs in the awake state ($90.30 \pm 5.03\%$, $n = 2,900$ cells in 11 mice) compared with the anesthetized state ($88.38 \pm 5.82\%$, $n = 702$ cells in 3 mice; ANOVA) (Fig. 1E). However, we observed a robust reduction of the synchronously firing populations under anesthesia ($55.87 \pm 11.38\%$), compared with awake mice ($95.35 \pm 3.67\%$, $P < 0.001$) (Fig. 1F). Therefore, USFs share similar mechanisms between awake and anesthetized conditions but anesthesia shows strong inhibitory effects on the generation of neuronal synchronicity.

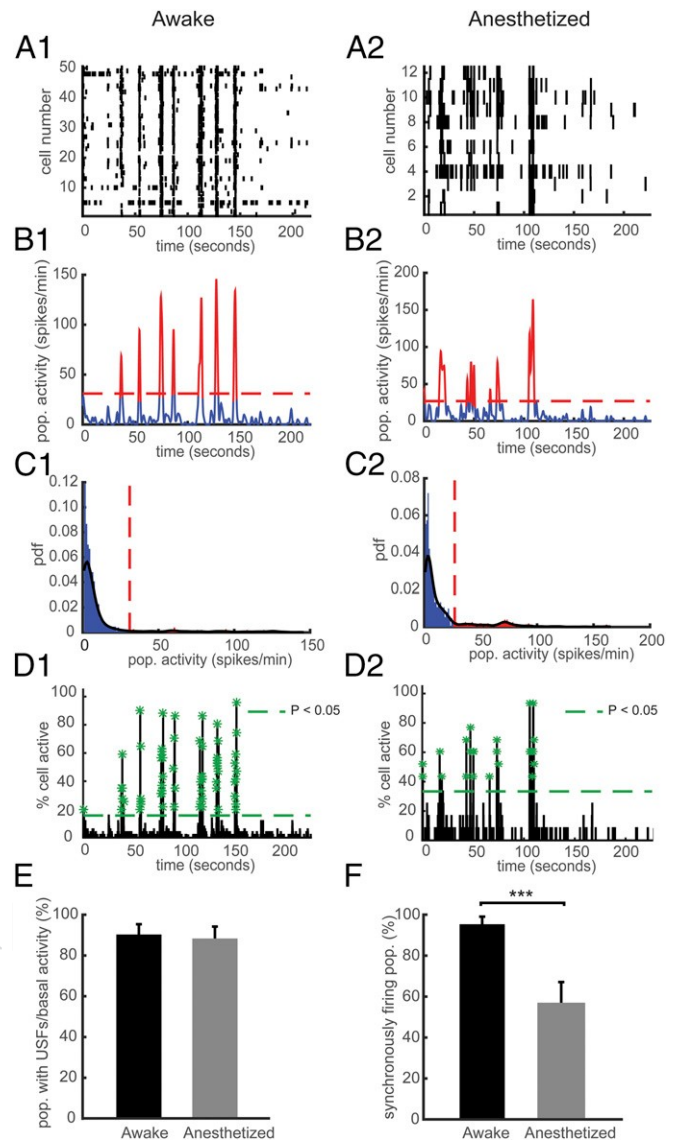


Fig. 1. Effect of general anesthesia on USFs and synchronously firing neurons in WT mice. (A) Representative rasterplots for one population of simultaneously recorded neurons in a WT mouse in the awake (A1) and anesthetized state (A2). Each row corresponds to the spiking activity of one neuron. (B) Mean neural activity for the populations in A in the awake (B1) and anesthetized state (B2). Red and blue correspond to USFs and basal activity states, respectively. Dotted red line: computed threshold. (C) Probability density function (pdf) of the population activity exhibited in B in the awake (C1) and anesthetized state (C2) for determining the threshold (red dotted line) between USFs and basal activity. Black line: Gaussian smoothed pdf, red bars: USFs and blue bars: basal activity. (D) Histogram representing the percentage of cells active in small time bins (~ 0.144 s), for the population activity in A in the awake (D1) and anesthetized state (D2). Asterisks: significant peaks of synchrony. (E) Computed percentage of cells exhibiting USFs. (F) Percentage of populations with synchronous activity in the awake and anesthetized state. (A1–D1) Awake, $n = 2,900$ cells in 11 mice, and (A2–D2) anesthetized, $n = 702$ cells in 3 mice.

Differential Role of nAChRs in the Generation of USFs and Synchronicity in the Awake State. Many studies in both animal models and humans have identified a contribution of nAChRs to cognitive functions; we thus investigated the occurrence of USFs transitions in KO mice of $\alpha 7$ and $\beta 2$ nAChR subunits. Typical examples of neuronal population activities in awake $\alpha 7$ and $\beta 2$ KO mice are shown in Fig. 2. We found that $90.30 \pm 5.03\%$ of simultaneously recorded populations exhibited USFs/basal activity

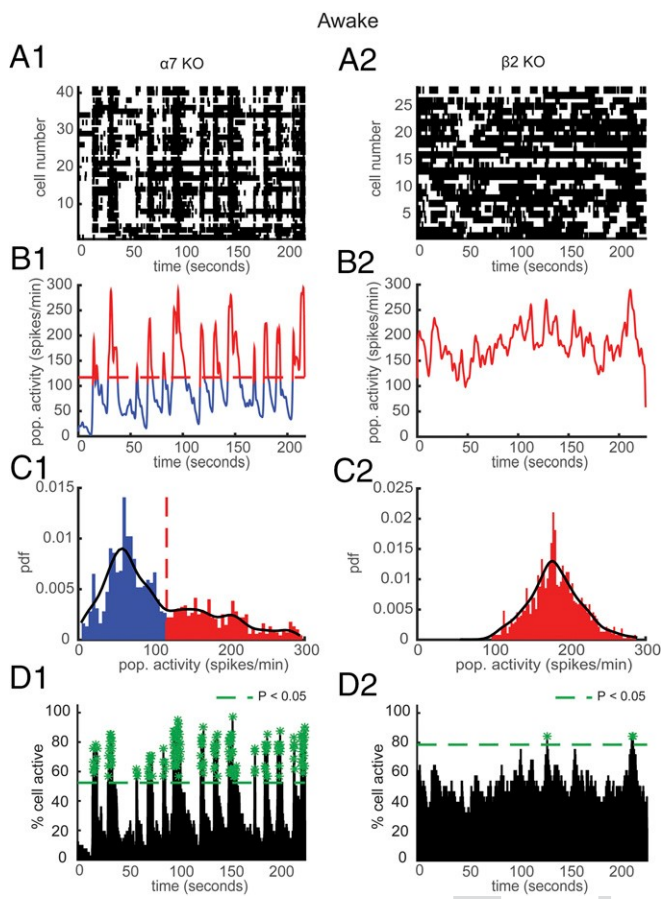


Fig. 2. Consequences of the $\alpha 7$ and $\beta 2$ nAChR deletion on USFs and synchronously firing neurons in the awake state. (A) Representative rasterplots for one population of simultaneously recorded neurons in $\alpha 7$ (A1) and $\beta 2$ (A2) KO awake mice. Each row corresponds to the spiking activity of one neuron. (B) Mean neural activity for the populations in A in $\alpha 7$ (B1) and $\beta 2$ (B2) KO awake mice. Red and blue correspond to USFs and basal activity states, respectively. Dotted red line: computed threshold. (C) Probability density function (pdf) of the population activity exhibited in B in $\alpha 7$ (C1) and $\beta 2$ (C2) KO awake mice for determining the threshold (red dotted line) between USFs and basal activity. Black line: Gaussian smoothed pdf, red bars: USFs and blue bars: basal activity. (D) Histogram representing the percentage of cells active in small time bins (~ 0.144 s), for the population activity in A in $\alpha 7$ (D1) and $\beta 2$ (D2) KO awake mice. Asterisks: significant peaks of synchrony. (A1–D1) $\alpha 7$ KO and (A2–D2) $\beta 2$ KO mice.

in WT ($n = 2,900$ cells in 11 mice), $82.08 \pm 7.2\%$ in $\alpha 7$ KO mice ($n = 1,403$ cells in 5 mice), and $65.86 \pm 5.7\%$ in $\beta 2$ KO mice ($n = 3,459$ cells in 11 mice) with a significant difference between WT and $\beta 2$ KO groups ($P = 0.0130$, ANOVA) (Fig. S2 A1). In each population of simultaneously recorded neurons with USFs/basal activity transitions, we determined the percentage of cells that exhibit an activity pattern in accordance with the population activity. In awake WT animals, $96.6 \pm 1.8\%$ of cells fire in accordance with their population activity, in $\alpha 7$ KO mice ($88.23 \pm 4.12\%$) and in $\beta 2$ KO mice ($84.37 \pm 2.27\%$) (Fig. S2 B1). To compute the percentage of cells with USFs/basal activity for each mouse group, we multiplied the percentage of populations with USFs/basal activity with the mean percentage of cells in accordance with the population patterns of activity, for each mouse. Interestingly, we found that $82.41 \pm 5.28\%$ of simultaneously recorded cells exhibited USFs in WT, $69.31 \pm 7.4\%$ in $\alpha 7$ KO mice, and $54.85 \pm 5.9\%$ in $\beta 2$ KO mice, with a significant difference between WT and $\beta 2$ KO mice ($P = 0.007$) (Fig. 3A).

Next, we computed the USFs/basal activity properties in all populations. The basal activity duration was significantly lower for the $\beta 2$ KO mice (7.36 ± 1.19 s), compared with $\alpha 7$ KO ($11.69 \pm$

2.43 s, $P = 0.0021$) and WT mice (14.43 ± 1.54 s, $P < 0.001$) (Fig. 3B), whereas the USFs duration was significantly higher for the $\beta 2$ KO mice (5.11 ± 0.64 s), compared with $\alpha 7$ KO (3.89 ± 0.65 s, $P = 0.0022$) and WT mice (3.03 ± 0.38 s, $P < 0.001$, Kruskal–Wallis) (Fig. 3C). Furthermore, computing the correlation between power spectra for each neuronal population for the different mice conditions in the awake state revealed that there are significantly lower correlations for $\beta 2$ KO compared with WT mice (Fig. S3). These data indicate that the USFs of each cell in a population of simultaneously recorded cells are more homogeneous in the case of WT and $\alpha 7$ KO mice compared with $\beta 2$ KO mice.

We then analyzed and compared the synchronicity in the different animal groups. In the WT and $\alpha 7$ KO mice, neurons displayed strong synchronous activity in $95.35 \pm 3.67\%$ (40 populations) and $88.33 \pm 11.66\%$ (38 populations) of the recorded populations, respectively, with no significant difference between groups ($P = 0.70$, ANOVA) (Fig. 3D). In the $\beta 2$ KO mice, the patterns of activity were remarkably different from that in WT ($P < 0.001$) and $\alpha 7$ KO mice ($P = 0.046$), with synchronous activity detected in only $63.91 \pm 5.38\%$ of the recorded populations (99 populations) (Fig. 3D). The number of synchrony peaks detected was similar between WT mice (30.59 ± 3.73 peaks per minute) and $\alpha 7$ KO mice (31 ± 6.77 peaks per minute, $P = 0.99$), whereas a robust decrease was observed in the case of $\beta 2$ KO mice (4.52 ± 0.72 peaks per minute, $P < 0.001$, ANOVA) (Fig. 3E). In addition, the percentage of coactive cells in the peaks of synchrony was significantly higher for $\alpha 7$ KO ($53.34 \pm 0.51\%$) and $\beta 2$ KO mice ($53.30 \pm 1.05\%$) compared with the WT mice ($47.71 \pm 0.47\%$, $P < 0.001$) (Fig. 3F).

Overall, USFs were still detected in mice with deleted nAChR subunits. However, $\beta 2$ KO mice showed reductions in the percentage of cells that exhibit USFs and a strong decrease in the percentage of synchronously firing neuronal populations. These data indicate a potentially major role for $\beta 2$ subunits in the generation of physiological phenomena associated with conscious processing in the awake state.

Role of nAChRs in Ongoing Activity Under General Anesthesia. The nAChRs are possible direct/indirect targets of general anesthetics and as a consequence may interfere with cholinergic transmission. For example, the volatile anesthetic isoflurane shows high affinity for nAChRs (34). However, isoflurane inhibition has been found to vary with nAChR subunit composition (35). We aimed to study in vivo the contribution of defined

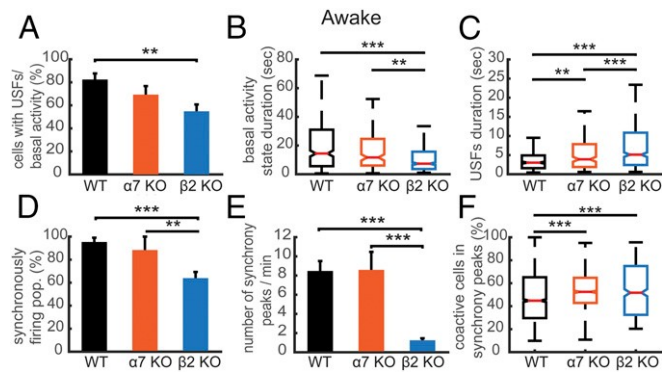


Fig. 3. Comparison of the properties of USFs and synchronicity in awake mice. (A) Percentage of cells with USFs for each animal type in the awake state. (B) Boxplots of basal activity durations for each animal type in the awake state. (C) Boxplots of USFs durations for each animal type. (D) Percentage of populations exhibiting synchronous activity for each mouse type in the awake state. (E) Mean number of synchrony peaks per minute for the different animal groups in the awake state. (F) Percentage of coactive cells in the peaks of synchrony for the different animal groups in the awake state. For all comparisons: * $P < 0.05$, ** $P < 0.01$, and *** $P < 0.001$; ANOVA in A, D, E, and F; Kruskal–Wallis in B and C.

373
374
375
376
377
378
379
380
381
382
383
384
385
386
387
388
389
390
391
392
393
394
395
396
397
398
399
400
401
402
403
404
405
406
407
408
409
410
411
412
413
414
415
416
417
418
419
420
421
422
423
424
425
426
427
428
429
430
431
432
433
434

Anesthetized

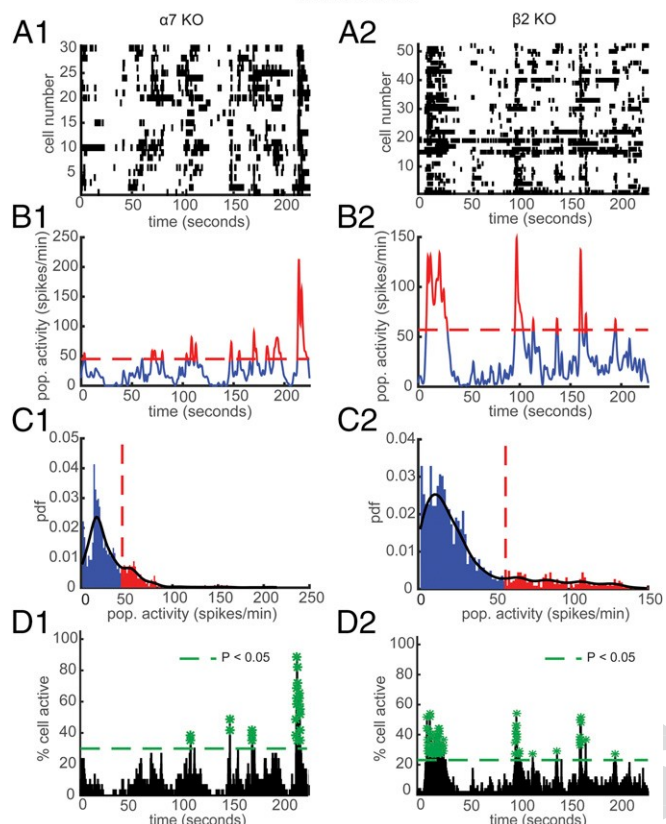


Fig. 4. Effect of general anesthetic on USFs and synchronously firing neurons in $\alpha 7$ and $\beta 2$ KO mice. (A) Representative rasterplots for one population of simultaneously recorded neurons in $\alpha 7$ (A1) and $\beta 2$ KO (A2) anesthetized mice. (B) Mean neural activity for the populations in A in $\alpha 7$ (B1) and $\beta 2$ KO (B2) anesthetized mice. Red and blue correspond to USFs and basal activity states, respectively. Dotted red line: computed threshold. (C) Probability density function (pdf) of the population activity in B in $\alpha 7$ (C1) and $\beta 2$ KO (C2) anesthetized mice. (D) Histogram representing the percentage of cells active in small time bins (~ 0.144 s) for the population activity in A in $\alpha 7$ (D1) and $\beta 2$ KO (D2) anesthetized mice. Asterisks: significant peaks of synchrony. (A1–D1) $\alpha 7$ KO and (A2–D2) $\beta 2$ KO mice.

nAChR subunits to spontaneous activity under conditions of light general anesthesia. Typical examples of the effect on the neuronal population activity in $\alpha 7$ and $\beta 2$ KO anesthetized mice are shown in Fig. 4. We found that $88.4 \pm 5.8\%$ of simultaneously recorded populations exhibited USFs/basal activity in WT mice, $76.6 \pm 14.5\%$ in $\alpha 7$ KO mice, and $85.7 \pm 4.9\%$ in $\beta 2$ KO mice, with no significant difference between the groups (Fig. S2 A2). Furthermore, in WT mice $96.42 \pm 4.28\%$ of cells fire in accordance with their population activity, $91.66 \pm 6.55\%$ in $\alpha 7$ KO mice, and $83.82 \pm 2.2\%$ in $\beta 2$ KO mice (Fig. S2 B2).

We also found that $76.68 \pm 4.35\%$ of simultaneously recorded cells exhibited USFs in WT mice, $65.89 \pm 14.16\%$ in $\alpha 7$ KO mice, and $68.35 \pm 4.3\%$ in $\beta 2$ KO mice, with no significant difference (Fig. 5A). Next, we computed the USFs/basal activity properties in all populations. Under anesthesia, there were no significant changes of basal activity state duration between animal types ($P > 0.14$, Kruskal–Wallis), nor any significant changes in variability ($P > 0.49$, Ansari–Bradley) (Fig. 5B). Conversely, the USF duration was significantly higher for the $\alpha 7$ KO mice (4.19 ± 2.57 s) and $\beta 2$ KO mice (2.86 ± 0.55 s), compared with WT mice (2.11 ± 0.40 s, $P < 0.001$) (Fig. 5C). In addition, there were no significant differences in the correlations of power spectra between the different mouse types in the anesthetized state (Fig. S3). For anesthetized animals, the number of simultaneously imaged cells in the same focal plane ranged from 3 to 96 neurons, with a

mean value of 23 neurons. Of simultaneously recorded populations, $55.87 \pm 11.38\%$ exhibited synchronous activity in WT mice (54 populations), $56.66 \pm 23.33\%$ in $\alpha 7$ KO mice (25 populations), and $65.41 \pm 18.20\%$ in $\beta 2$ KO mice (129 populations), with no significant differences ($P > 0.9$) between groups (Fig. 5D). Interestingly, in the anesthetized state, the number of synchrony peaks detected was similar between WT mice (0.79 ± 0.16 peaks per minute) and $\alpha 7$ KO mice (1.41 ± 0.52 peaks per minute), whereas a robust increase was observed in the case of $\beta 2$ KO mice (4.58 ± 0.62 peaks per minute, $P < 0.001$) (Fig. 5E). Finally, the percentage of coactive cells in the peaks of synchrony was significantly higher for the WT mice ($41.03 \pm 1.03\%$) and $\alpha 7$ KO mice ($46.30 \pm 1.25\%$) compared with $\beta 2$ KO mice ($21.74 \pm 0.19\%$, $P < 0.001$, ANOVA) (Fig. 5F). To summarize these results, the deletion of nAChR $\alpha 7$ and $\beta 2$ subunits has differential effects in awake mice on USFs duration, whereas in the anesthetized state, $\beta 2$ deletion alone increases synchronicity and decreases the percentage of coactive cells in the peaks of synchrony, compared with WT and $\alpha 7$ KO mice.

Chronic Exposure to Mecamylamine Mimics $\beta 2$ KO Phenotype. Finally, we aimed to compare the neuronal activity patterns in the PFC of WT mice after chronic application of mecamylamine, a non-selective, noncompetitive antagonist of nAChRs. Osmotic minipumps for the infusion of either saline or mecamylamine (1 mg/kg per day for mecamylamine) were implanted subcutaneously at the nape of the neck of WT mice. We recorded the neuronal activity patterns 7 d after minipump implantation. Typical examples of neuronal population activities in awake mice under saline or mecamylamine are shown in Fig. S4. We found that $94.44 \pm 5.55\%$ of simultaneously recorded populations exhibited USFs/basal activity in WT under saline condition ($n = 743$ cells in 3 mice) and $69.44 \pm 2.77\%$ in WT under mecamylamine ($n = 446$ cells in 3 mice) with a significant difference between the two groups ($P = 0.015$) (Fig. S5A). In awake WT animals under saline conditions, $98.21 \pm 2.4\%$ of cells fire in accordance with their population activity, whereas in WT under mecamylamine $90.32 \pm 2.4\%$ of cells were in accordance ($P = 0.041$) (Fig. S5B). In addition, we found that $88.91 \pm 3.67\%$ of simultaneously recorded cells exhibited USFs in WT under saline, whereas a significant reduction was observed for the WT mice under mecamylamine ($62.28 \pm 3.18\%$, $P = 0.0054$) (Fig. 6 A1). The basal activity duration was significantly lower for the WT mice under mecamylamine (13.62 ± 3.97 s),

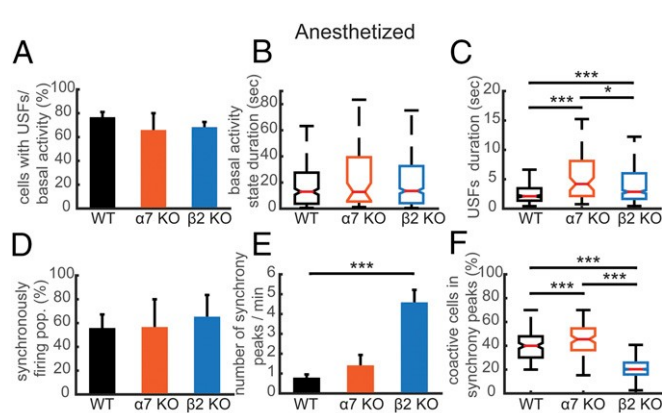


Fig. 5. Comparison of the properties of USFs and synchronicity in anesthetized mice. (A) Percentage of cells with USFs for each animal type in the anesthetized state. (B) Boxplots of basal activity durations for each animal type in the anesthetized state. (C) Boxplots of USFs durations for each animal type in the anesthetized state. (D) Percentage of populations with synchronous activity, for each mouse type in the anesthetized state. (E) Mean number of synchrony peaks per minute for the different animal group in the anesthetized state. (F) Percentage of coactive cells in the peaks of synchrony for each animal type in the anesthetized state. For all comparisons: $*P < 0.05$, $**P < 0.01$, and $***P < 0.001$; ANOVA in A, D, and E; Kruskal–Wallis in B and C.

435
436
437
438
439
440
441
442
443
444
445
446
447
448
449
450
451
452
453
454
455
456
457
458
459
460
461
462
463
464
465
466
467
468
469
470
471
472
473
474
475
476
477
478
479
480
481
482
483
484
485
486
487
488
489
490
491
492
493
494
495
496

497 compared with WT under saline (17.02 ± 4.18 s, $P = 0.018$) (Fig. 498 **S5C**). Furthermore, USF duration was significantly higher for WT 499 under saline (2.90 ± 0.28 s), compared with WT under mecamyli- 500 amine (1.95 ± 0.45 s, $P = 0.011$) (Fig. **S5D**).

501 We then analyzed and compared the synchronicity under saline 502 and mecamlamine infusion. In the WT mice under saline, neurons 503 displayed synchronous activity in $81.11 \pm 11.60\%$ of the recorded 504 populations, whereas in WT mice under mecamlamine $88.89 \pm 505 11.11\%$ of the recorded populations had synchronous activity, with 506 no significant difference between groups ($P = 0.65$) (Fig. **S5E**). 507 However, the number of synchrony peaks detected was strongly 508 decreased in WT mice under mecamlamine (3.27 ± 1.09 peaks per 509 minute) in comparison with WT mice under saline (17 ± 4.94 peaks 510 per minute, $P = 0.036$) (Fig. 6 **A, 2**). In addition, the percentage of 511 coactive cells in the peaks of synchrony was significantly lower for 512 WT under mecamlamine ($21.86 \pm 0.80\%$) compared with the WT 513 mice under saline ($28.64 \pm 0.8\%$, $P < 0.001$) (Fig. **S5F**). Thus, 514 pharmacological exposure to the nicotinic antagonist mecamlamine 515 gives a phenotype similar to that found in $\beta 2$ KO mice.

516 Discussion

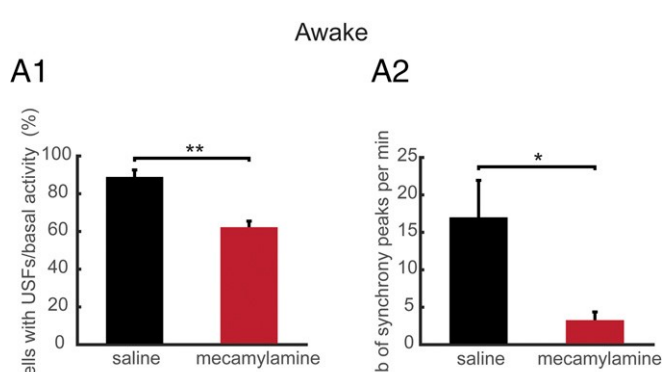
517 In humans, two distinct modes of electrical activation of the cere- 518 bral cortex have been recorded: a rapid and sustained activation, 519 termed “ignition,” which is viewed as a signature of conscious ac- 520 cess; and synchronous USFs with low amplitude, which characterize 521 the spontaneous activity mode, termed “resting state” (19). In the 522 resting state, in the absence of explicit task performance or external 523 stimulus perception, the cortex exhibits a highly informative mode 524 of spontaneous activity. Studies in anesthetized animals (21) and in 525 humans with blood-oxygen level-dependent fMRI data (27), to- 526 gether with animal recordings of firing-rate modulations (23), and 527 EEG (22) and ECoG in humans (23, 36), reveal ultraslow (<0.1 Hz) 528 dynamic activations with low amplitude, that we termed USFs, 529 which may be viewed as characterizing the resting state. Here, we 530 aimed to elucidate the mechanisms engaged in these cortical ac- 531 tivity dynamics at a single-cell resolution using *in vivo* two-photon 532 imaging in the mouse. We recorded ongoing spontaneous activity in 533 the PFC of WT and mice deleted for specific nAChR subunits, both 534 in awake and anesthetized states. Interestingly, we recorded USFs 535 in the mouse cortex and found that anesthesia shows inhibitory 536 effects by disrupting the synchronous USFs’ firing of neurons. We 537 further showed that, first, nAChRs have an important role in the 538 generation of USFs, yet to a different extent during quiet wake- 539 fulness and anesthesia, and that the $\beta 2$ subunit is specifically re- 540 quired for synchronized activity patterns. Our recordings indicate 541 that, similar to humans, the ongoing activity in mouse brain con- 542 stantly fluctuates and exhibits synchronously firing neuronal activity,

making the mouse a reliable, although simplified model, for 502 studying mechanisms of conscious processing in humans.

503 Current theories consider the PFC as a key player in conscious 504 processing (6). According to the Global Neuronal Workspace 505 (GNW) theory, a subset of cortical pyramidal cells with long- 506 range excitatory axons that are particularly dense in prefrontal, 507 cingulate, and parietal regions, together with the relevant tha- 508 lamo-cortical loops, form a horizontal “neuronal workspace” 509 interconnecting the multiple specialized, automatic, and non- 510 conscious processors. A conscious content is assumed to be 511 encoded by the “all or none” sustained and synchronous ignition 512 of a fraction of GNW neurons (7, 8). In these circumstances, the 513 nonamplified neurons would be inhibited and the GNW sus- 514 tained ignition would represent the conscious content. In the 515 PFC, pyramidal neurons in layer II/III do not express nAChRs, 516 only interneurons do, in contrast to layers V and VI, where 517 nAChRs are also expressed by pyramidal neurons (37). In addi- 518 tion, pyramidal neurons with long axons, which have been postu- 519 lated to play a critical role in the GNW theory (38), are more 520 abundant in these particular layers of the cerebral cortex and es- 521 pecially in the PFC (39). By recording neuronal activity patterns in 522 layer II/III of PFC, we found that $\alpha 7$ and $\beta 2$ nAChRs play an 523 important role in the generation of USFs that occur, yet to a 524 different extent during quiet wakefulness and anesthesia. We 525 showed that the balance of recurrent excitation and inhibition is 526 disrupted in the case of awake $\beta 2$ KO mice, and more specifically, 527 the neuronal synchronicity is disrupted. It has been reported that $\beta 2$ 528 subunit is involved in the dendritic morphogenesis of pyra- 529 midal neurons, and in particular, in the circuits that contribute 530 to the high-order functional connectivity of the cerebral cortex 531 (40). These defects in the maturation of the cerebral cortex that 532 have been reported in the $\beta 2$ KO mice could contribute to the 533 observed behavioral deficits (4, 13, 16). However, our data reveal 534 that pharmacological intervention with nicotinic antagonists is 535 enough for the disruption of USF mechanisms. Our findings 536 suggest an important contribution of nAChRs in the processing of 537 neural information during quiet wakefulness.

538 Moreover, an important role of the cholinergic innervation of 539 the cerebral cortex was postulated (41) to be the mediation of 540 arousal state. This hypothesis was based on the initial observa- 541 tion that the cholinergic inputs are diffusely distributed in the 542 cerebral cortex and, most interestingly for us, exhibits a slow 543 release of ACh on the same time scale as the USFs. Several 544 studies have further shown that cholinergic projections to the 545 cortex are involved in sustained attention and cue detection, with 546 the level of ACh efflux in the PFC correlating with the demand 547 upon attention during attentional tasks (42). The slow fluctua- 548 tions in ACh levels correlate with a shift in behavior, indicating 549 that these fluctuations could correlate with decision-making (42, 550 43). Indeed, experimental evidence from both rodents and hu- 551 mans revealed that ACh release contributes to mechanisms that 552 mediate the integration of external cues with internal represen- 553 tations to initiate and guide behavior (44). At the scale of sec- 554 onds, ACh undergoes phasic release, which may exert a top- 555 down control over defined cognitive operations; muscarinic ACh 556 receptors also play an important role in attentional behavior and 557 cue detection (45). Recently, it has been shown *in vitro* that 558 endogenously released ACh can modulate up and down states 559 through the activation of nAChRs (46). The alterations of neu- 560 ronal activity patterns that our results revealed in the nAChR 561 KO mice could further our understanding of the cholinergic 562 system in higher brain functions and, when disrupted, the con- 563 tribution of nAChRs to cognitive disorders.

564 The focus of the present study was to elucidate the role of 565 nAChRs in PFC activity patterns when comparing resting-state 566 dynamics in awake and anesthetized animals. Because ongoing 567 spontaneous activity has been postulated to have a significant 568 functional role in cortical functions (47), we focused on how it 569 differs between awake and anesthetized states. The production 570 of USFs was identified and compared among the different con- 571 ditions investigated. Our work demonstrates, *in vivo*, that nAChRs



542 Fig. 6. Chronic exposure to mecamlamine mimics $\beta 2$ KO phenotype. (A1) 543 Percentage of populations that exhibit USFs for awake WT mice under saline 544 or mecamlamine conditions at 7 d after implantation of minipumps. (A2) 545 Mean number of synchrony peaks per minute for awake WT mice under saline 546 or mecamlamine infusion 7 d after implantation of minipumps. * $P < 0.05$, 547 ** $P < 0.01$, and *** $P < 0.001$; ANOVA.

621 play a crucial role in the modulation of PFC synchronous spon- 683
622 taneous neuronal activity. Furthermore, with recent studies 684
623 probing the mechanisms of general anesthesia as causing loss of 685
624 consciousness, our work exploring the effects of anesthesia on 686
625 nAChRs in the PFC network *in vivo*, at a cellular resolution, re- 687
626 veals an elaborate mechanism for modulating cortical activity. Our 688
627 results provide a starting point for understanding the relationship 689
628 between nAChRs and loss of consciousness under light anesthesia 690
629 in mice that might potentially be a reliable—although highly 691
630 simplified—model for studying mechanisms of conscious pro- 692
631 cessing in humans. As a future goal, it is important to consider 693
632 additional studies to evaluate the presence of USFs during be- 694
633 havioral assays. Because several studies have shown that deletion 695
634 in mice of the $\alpha 7$ and $\beta 2$ subunits impairs behaviors, such as ex- 696
635 ploratory behavior and attention, it will be important to investigate 697
636 the behavioral deficits in parallel with neuronal recordings to es- 698
637 tablish a causal relationship. 699

637 Materials and Methods

638 Male $\alpha 7$ KO, $\beta 2$ KO, and WT (C57BL/6J) mice used in this study were main- 700
639 tained at Charles River Laboratories (L'Arbresle, France). The experiments 701

- 640 1. Dalley JW, Cardinal RN, Robbins TW (2004) Prefrontal executive and cognitive functions 702
641 in rodents: neural and neurochemical substrates. *Neurosci Biobehav Rev* 28(7):771–784. 703
- 642 2. Khan ZU, Muly EC (2011) Molecular mechanisms of working memory. *Behav Brain Res* 704
643 219(2):329–341. 705
- 644 memory and decision making. *Neuron* 76(6):1057–1070. 706
- 645 4. Avale ME, et al. (2011) Prefrontal nicotinic receptors control novel social interaction 707
646 between mice. *FASEB J* 25(7):2145–2155. 708
- 647 5. Miller EK (2000) The prefrontal cortex and cognitive control. *Nat Rev Neurosci* 1(1): 709
648 59–65. 710
- 649 6. Dehaene S, Changeux J-P (2011) Experimental and theoretical approaches to consci- 711
650 ous processing. *Neuron* 70(2):200–227. 712
- 651 7. Koch C, Massimini M, Boly M, Tononi G (2016) Neural correlates of consciousness: 713
652 Progress and problems. *Nat Rev Neurosci* 17(5):307–321. 714
- 653 8. Changeux J-P (2012) Conscious processing: Implications for general anesthesia. *Curr 715
654 Opin Anaesthesiol* 25(4):397–404. 716
- 655 9. Poorthuis RB, Mansvelder HD (2013) Nicotinic acetylcholine receptors controlling atten- 717
656 tion: Behavior, circuits and sensitivity to disruption by nicotine. *Biochem 718
657 Pharmacol* 86(8):1089–1098. 719
- 658 10. Granon S, Changeux J-P (2012) Deciding between conflicting motivations: what mice 720
659 make of their prefrontal cortex. *Behav Brain Res* 229(2):419–426. 721
- 660 11. Koukoulis F, Maskos U (2015) The multiple roles of the $\alpha 7$ nicotinic acetylcholine 722
661 receptor in modulating glutamatergic systems in the normal and diseased nervous 723
662 system. *Neurosci Biobehav Rev* 49:103–117. 724
- 663 12. Picciotto MR, et al. (1995) Abnormal avoidance learning in mice lacking functional 725
664 high-affinity nicotine receptor in the brain. *Nature* 374(6517):65–67. 726
- 665 13. Maskos U, et al. (2005) Nicotine reinforcement and cognition restored by targeted 727
666 expression of nicotinic receptors. *Nature* 436(7047):103–107. 728
- 667 14. Hoyle E, Genn RF, Fernandes C, Stolerman IP (2006) Impaired performance of alpha7 729
668 nicotinic receptor knockout mice in the five-choice serial reaction time task. 730
669 *Psychopharmacology (Berl)* 189(2):211–223. 731
- 670 15. Naudé J, et al. (2016) Nicotinic receptors in the ventral tegmental area promote 732
671 uncertainty-seeking. *Nat Neurosci* 19(3):471–478. 733
- 672 16. Guillem K, et al. (2011) Nicotinic acetylcholine receptor $\beta 2$ subunits in the medial 734
673 prefrontal cortex control attention. *Science* 333(6044):888–891. 735
- 674 17. Fox MD, Raichle ME (2007) Spontaneous fluctuations in brain activity observed with 736
675 functional magnetic resonance imaging. *Nat Rev Neurosci* 8(9):700–711. 737
- 676 18. Moutard C, Dehaene S, Malach R (2015) Spontaneous fluctuations and non-linear 738
677 ignitions: Two dynamic faces of cortical recurrent loops. *Neuron* 88(1):194–206. 739
- 678 19. Dehaene S, Changeux J-P (2005) Ongoing spontaneous activity controls access to 740
679 consciousness: A neuronal model for inattention blindness. *PLoS Biol* 3(5):e141. 741
680 neocortex. *Nature* 423(6937):283–288. 742
- 681 21. Arieli A, Sterkin A, Grinvald A, Aertsen A (1996) Dynamics of ongoing activity: 743
682 Explanation of the large variability in evoked cortical responses. *Science* 273(5283): 744
1868–1871. 745
- 683 22. Schurger A, Sarigiannidis I, Naccache L, Sitt JD, Dehaene S (2015) Cortical activity is 746
684 more stable when sensory stimuli are consciously perceived. *Proc Natl Acad Sci USA* 747
685 112(16):E2083–E2092. 748
- 686 23. Nir Y, et al. (2008) Interhemispheric correlations of slow spontaneous neuronal fluc- 749
687 tuations revealed in human sensory cortex. *Nat Neurosci* 11(9):1100–1108. 750
- 688 24. Bartfeld P, et al. (2015) Signature of consciousness in the dynamics of resting-state 751
689 brain activity. *Proc Natl Acad Sci USA* 112(3):887–892. 752
- 690 25. Deco G, Haggmann P, Hudetz AG, Tononi G (2014) Modeling resting-state functional 753
691 networks when the cortex falls asleep: Local and global changes. *Cereb Cortex* 24(12): 754
3180–3194. 755
- 692 26. Raichle ME, et al. (2001) A default mode of brain function. *Proc Natl Acad Sci USA* 756
693 98(2):676–682. 757

described in this study were conducted in accordance with the guidelines on 683
the ethical use of animals from the European Community Council Directive of 684
November 24, 1986 (86/609/EEC) and in accordance with institutional animal 685
welfare guidelines and were approved by Animalerie Centrale and Médecine 686
du Travail, Institut Pasteur. 687

Chronic cranial windows were performed as previously described (48) 688
and 200 nL of AAV.syn.GCaMP6f was injected bilaterally in the PFC. Two- 689
photon experiments were performed with an Ultima IV two-photon laser- 690
scanning microscope system (Bruker), at a frame rate of 7 Hz. For data 691
analysis we used ImageJ software and we developed a custom-written 692
toolbox in MATLAB. Full methods are described in *SI Materials and 693
Methods*. 694

ACKNOWLEDGMENTS. We thank David DiGregorio for maintaining the im- 695
aging platform of the Department of Neuroscience; Kurt Sailor for editing of 696
the manuscript; the GENIA Program and the Janelia Research Campus and Q:16 697
specifically Vivek Jayaraman, Douglas S. Kim, Loren L. Looger, and Karel 698
Svoboda from the GENIE Project, Janelia Research Campus, Howard Hughes 699
Medical Institute for making the GCaMP6 available. F.K. is a scholar of the 700
Pasteur Paris University Doctoral Program and received a stipend from the 701
Stavros Niarchos Foundation. 702

- 703 27. Biswal B, Yetkin FZ, Haughton VM, Hyde JS (1995) Functional connectivity in the 704
705 motor cortex of resting human brain using echo-planar MRI. *Magn Reson Med* 34(4): 706
153–169. 707
- 708 28. Vincent JL, et al. (2007) Intrinsic functional architecture in the anaesthetized monkey 709
710 brain. *Nature* 447(7141):83–87. 711
- 712 29. Nir Y, Hasson U, Levy I, Yeshurun Y, Malach R (2006) Widespread functional 713
714 connectivity and fMRI fluctuations in human visual cortex in the absence of visual stim- 715
716 ulation. *Neuroimage* 30(4):1313–1324. 717
- 718 30. Nir Y, et al. (2011) Regional slow waves and spindles in human sleep. *Neuron* 70(1): 719
720 153–169. 721
- 722 31. Cordes D, et al. (2001) Frequencies contributing to functional connectivity in the 723
724 cerebral cortex in “resting-state” data. *AJNR Am J Neuroradiol* 22(7):1326–1333. 725
- 726 32. Alkire MT, Hudetz AG, Tononi G (2008) Consciousness and anesthesia. *Science* 727
728 322(5903):876–880. 729
- 729 33. Goltstein PM, Montijn JS, Pennartz CMA (2015) Effects of isoflurane anesthesia on 730
731 ensemble patterns of Ca²⁺ activity in mouse v1: Reduced direction selectivity in- 732
733 dependent of increased correlations in cellular activity. *PLoS One* 10(2):e0118277. 734
- 735 34. Flood P, Role LW (1998) Neuronal nicotinic acetylcholine receptor modulation by 736
737 general anesthetics. *Toxicol Lett* 100-101:149–153. 738
- 739 35. Tassonyi E, Charpentier E, Muller D, Dumont L, Bertrand D (2002) The role of nicotinic 740
741 acetylcholine receptors in the mechanisms of anesthesia. *Brain Res Bull* 57(2):133–150. 742
- 743 36. He BJ, Snyder AZ, Zempel JM, Smyth MD, Raichle ME (2008) Electrophysiological 744
745 correlates of the brain’s intrinsic large-scale functional architecture. *Proc Natl Acad Sci 746
747 USA* 105(18):6382–6387. 748
- 749 37. Poorthuis RB, et al. (2013) Layer-specific modulation of the prefrontal cortex by ni- 749
750 cotinic acetylcholine receptors. *Cereb Cortex* 23(1):148–161. 751
- 752 38. Dehaene S, Kerszberg M, Changeux JP (1998) A neuronal model of a global work- 753
754 space in effortful cognitive tasks. *Proc Natl Acad Sci USA* 95(24):14529–14534. 755
- 756 39. Von Economo C (1929) The cytoarchitectonics of the human cerebral cortex *J Anat* 63 756
757 (Pt 3):389. 758
- 759 40. Ballesteros-Yáñez I, Benavides-Piccione R, Bourgeois J-P, Changeux J-P, DeFelipe J 759
760 (2010) Alterations of cortical pyramidal neurons in mice lacking high-affinity nicotinic 760
761 receptors. *Proc Natl Acad Sci USA* 107(25):11567–11572. 761
- 762 41. Parikh V, Sarter M (2008) Cholinergic mediation of attention: Contributions of phasic 762
763 and tonic increases in prefrontal cholinergic activity. *Ann NY Acad Sci* 1129:225–235. 763
- 764 42. Sarter M, Parikh V, Howe WM (2009) Phasic acetylcholine release and the volume 764
765 transmission hypothesis: Time to move on. *Nat Rev Neurosci* 10(5):383–390. 765
- 766 43. Parikh V, Kozak R, Martinez V, Sarter M (2007) Prefrontal acetylcholine release con- 766
767 trols cue detection on multiple timescales. *Neuron* 56(1):141–154. 767
- 768 44. Howe WM, et al. (2013) Prefrontal cholinergic mechanisms instigating shifts from 768
769 monitoring for cues to cue-guided performance: Converging electrochemical and 769
770 771 772 773 774 775 776 777 778 779 780 781 782 783 784 785 786 787 788 789 790 791 792 793 794 795 796 797 798 799 800

AUTHOR QUERIES

AUTHOR PLEASE ANSWER ALL QUERIES

1

- Q: 1_Please contact PNAS_Specialist.djs@sheridan.com if you have questions about the editorial changes, this list of queries, or the figures in your article. Please include your manuscript number in the subject line of all email correspondence; your manuscript number is 201614417.
- Q: 2_Please (i) review the author affiliation and footnote symbols carefully, (ii) check the order of the author names, and (iii) check the spelling of all author names, initials, and affiliations. Please check with your coauthors about how they want their names and affiliations to appear. To confirm that the author and affiliation lines are correct, add the comment “OK” next to the author line. This is your final opportunity to correct any errors prior to publication. Misspelled names or missing initials will affect an author’s searchability. Once a manuscript publishes online, any corrections (if approved) will require publishing an erratum; there is a processing fee for approved erratum.
- Q: 3_Please review and confirm your approval of the short title: Nicotinic receptors and spontaneous brain activity. If you wish to make further changes, please adhere to the 50-character limit. (NOTE: The short title is used only for the mobile app and the RSS feed.)
- Q: 4_Please review the information in the author contribution footnote carefully. Please make sure that the information is correct and that the correct author initials are listed. Note that the order of author initials matches the order of the author line per journal style. You may add contributions to the list in the footnote; however, funding should not be an author’s only contribution to the work.
- Q: 5_You have chosen not to pay an additional \$1350 (or \$1000 if your institution has a site license) for the PNAS open access option. Please confirm this is correct and note your approval in the margin.
- Q: 6_Please verify that all callouts for supporting information (SI) in text are correct. Note, however, that the hyperlinks for SI callouts will not work until the article is published online. In addition, SI that is not composed in the main SI PDF (appendices, datasets, movies, and “Other Supporting Information Files”) have not been changed from your originally submitted file and so are not included in this set of proofs. The proofs for any composed portion of your SI are included in this proof as subsequent pages following the last page of the main text. If you did not receive the proofs for your SI, please contact PNAS_Specialist.djs@sheridan.com.
- Q: 7_Please check the order of your keywords and approve or reorder them as necessary. Note that PNAS allows up to five keywords; please do not add new keywords unless you wish to replace others.
- Q: 8_Per PNAS style, certain compound terms are hyphenated when used as adjectives and unhyphenated when used as nouns. This style has been applied consistently throughout where (and if) applicable.
- Q: 9_Please provide a new title without the use of a colon.
- Q: 10_Please confirm whether all units, divisions, departments, laboratories, or sections have been included in the affiliations line for each footnote symbol or add if missing. PNAS requires smallest

AUTHOR QUERIES

AUTHOR PLEASE ANSWER ALL QUERIES

2

institutional unit(s) to be listed for each author in each affiliation. Please also provide a postal code for affiliation “c.”

Q: 11_Please verify the corresponding author email addresses as provided.

Q: 12_Original refs. 23 and 36 were identical and 37 and 22 were identical. As such, original refs. 36 and 37 have been renumbered as refs. 23 and 22, respectively. All subsequent references have been renumbered as refs. 36-51, respectively. Please check.

Q: 13_Does the edit preserve your intent? Please check the sentence beginning “We showed that the balance...”

Q: 14_PNAS requires that statements regarding the animal study protocols are cited in the main text. As such, this information has been copied from the SI and added to the main text Materials and Methods. Please check.

Q: 15_In the Acknowledgments, please check the names of persons thanked for assistance/contributions, names of granting agencies, grant numbers, and initials of grant recipients for accuracy.

Q: 16_PNAS articles should be accessible to a broad scientific audience. As such, please spell out “GENIA” and “GENIE,” if possible.

Q: 17_Please verify the author provided for ref. 39 and that it is only one page.

Q: 18_Does the edit preserve your intent? Please check the last line of Figs. 1, 2 and 4.

Q: 19_Please provide a value for the triple asterisks in Fig. 1F.

Q: 20_It has been assumed that the callouts for B1 and A2 in the legend for Fig. 2B should be for B1 and B2 instead. Please check.



Supporting Information

Koukouli et al. 10.1073/pnas.1614417113

SI Materials and Methods

Mice. All experiments were performed on male mice at 3 mo of age. Male $\alpha 7$ KO, $\beta 2$ KO, and WT (C57BL/6J) mice used in this study were maintained at Charles River Laboratories (L'Arbresle, France). The experiments described in this study were conducted in accordance with the guidelines on the ethical use of animals from the European Community Council Directive of November 24, 1986 (86/609/EEC) and in accordance with institutional animal welfare guidelines and were approved by Animalerie Centrale and Médecine du Travail, Institut Pasteur.

Chronic Cranial Windows and Stereotaxic Injections. Anesthesia was induced with ketamine (Imalgen 1000; Rhone Mérieux) and xylazine (Rompun; Bayer AG), 10 mL/kg, intraperitoneally, and the mouse was secured in a stereotaxic frame. The eyes were protected with artificial tear ointment and body temperature was maintained with a feedback-heating pad. The scalp was washed thoroughly with betadine and 70% ethanol and all surgical tools were sterilized. Xylocaine (1%) was used for local anesthesia and the skull was exposed. As previously described (48), a chronic cranial window was prepared and 200 nL of [serotype 1 (rep/cap: 2/1)] AAV virus (AAV.syn.GCaMP6f.WPRE.SV40, 2.2×10^{13} GC/mL; University of Pennsylvania Vector Core) was injected bilaterally at the following coordinates PrLC: AP, +2.8 mm from bregma; L, ± 0.5 mm; and DV, -0.5 to -0.1 mm from the skull using a Nanoject II (Drummond Scientific) at the slow infusion setting. The glass pipette was left for 5 min in the brain before slowly being removed. A 5-mm-diameter circular coverglass was placed on the brain surface and the edge was sealed to the skull with dental cement (Coffret SUPERBOND complete, Phymep). A sterile small stainless steel head bar with a screw hole was glued to the skull and the surrounding exposed skull was covered with dental cement.

Mouse Handling for Awake Imaging. For 3–5 d mice were habituated to the imaging environment by handling and training, as previously described (49).

Immunofluorescence. Immunofluorescence was performed to identify the area of injection at the end of the two-photon imaging experiments. Mice were transcardiac-perfused with 4% PFA, the brains were removed and postfixed with immersion in PFA for 2 d at 4 °C, followed by immersion in 30% sucrose in PBS overnight for cryoprotection. Using a sliding microtome (Leica Microsystems), serial 40- μ m coronal sections were cut, mounted on slides, and cover-slipped with ProLong Gold antifade reagent containing DAPI (Invitrogen). Microscopy was carried out using a Zeiss fluorescence microscope.

In Vivo Two-Photon Imaging. In vivo imaging was performed with an Ultima IV two-photon laser-scanning microscope system (Bruker), using a 16×0.8 NA water immersion objective (Nikon) with a femtosecond laser (MaiTai DeepSee, Spectra Physics) tuned to 950 nm for imaging of GCaMP6f-expressing cells. Time-series movies of neuronal populations expressing GCaMP6f were acquired at 7 Hz ($182 \times 182 \mu\text{m}$ field of view; $0.71 \mu\text{m}$ per pixel). Each focal plane movie duration was 3.6 min (1,500 frames) to track the spontaneous neuronal activity. For anesthetized mice, recordings were conducted under light isoflurane anesthesia (0.8% isoflurane in O_2).

Recordings in Anesthetized Mice. The mouse was placed into a transparent induction chamber (Harvard Apparatus) and anesthesia was induced at a concentration of 5% vaporized iso-

flurane/ O_2 (Forene, Abbott France; vaporizer, Harvard Apparatus) leading to a rapid induction of anesthesia within 30 s, as tested by loss of righting reflex and pain with a tail pinch. The mouse was then removed from the induction chamber and immediately secured to the mouse frame on the two-photon microscope stage. The mice were continuously supplied with 0.8% isoflurane/ O_2 through a facemask. Body temperature was maintained at 37 °C using a thermometer feedback thermal blanket. Artificial tear ointment was also applied to the eyes to prevent dryness. The recordings started ~15 to 20 min after placing the animal on the stage and anesthesia was maintained constant until the end of the experiments, as previously described (33). Under these conditions the mice were completely immobile, had no reaction to tail pinch, and eyelid reflex was absent.

Data Analysis. Image analysis was performed off-line with ImageJ software. The time series were corrected using the FIJI plugin “Image Stabilizer” (K. Li, “The image stabilizer plugin for ImageJ,” www.cs.cmu.edu/~kangli/code/Image_Stabilizer.html). Regions of interest were manually selected in FIJI and detection of Ca^{2+} transients of individual neurons was performed automatically using a custom-written toolbox in MATLAB. A baseline correction algorithm was used to remove the slow time scale (< 0.05 Hz) changes in the fluorescence, as described previously (50). We assumed the smallest and fastest Ca^{2+} transients were a result of a single action potential. The mean shape and amplitude of this unitary event was used as a kernel for deconvolution to best estimate action potential or spike frequency. The custom-written toolbox in MATLAB (Mathworks, 2014b) is available upon request.

For the analysis of USFs, the time-varying population activity was computed as the mean activity across neurons for each time bin, and was smoothed through Gaussian filtering. The distribution (pdf estimate) of the activity values was plotted at each time point that exhibits multimodality or unimodality. To identify the type of modality of the distribution, we used Gaussian filtering (black lines in Fig. 1C). The number of peaks determined the types of activity: multiple peaks are the signatures for USFs vs. basal activity states. The threshold between USFs vs. basal activity states was computed by taking the minimum of the multimodal distributions between the highest amplitude peak and its neighboring peak (red dotted lines in Fig. 1C). In some cases, where one of the activity states was very short (in the case of WT), a Gaussian or logistic function could be fitted around the highest amplitude peak (according to the root mean-square error output), and the activity state with low durations could be identified by taking values $> 99\%$ or $< 1\%$ of the cumulative sums. The USFs correspond to population activities in red, and basal activities correspond to population activities in blue (Fig. 3C). Our analysis method is based on a previously described technique (51).

We identified synchronously firing neurons based on a method that was previously described (20). For each population, small time bins (~ 0.144 s) were used to sum the spiking activity of all of the cells. To identify peaks of synchronous activity that included more cells than expected by chance, interval reshuffling (randomly reordering of intervals between events for each cell) was used to create sets of event sequences. Reshuffling was carried out 1,000 times for each population and a histogram was constructed for each reshuffling. The threshold corresponding to a significant level of $P < 0.05$ (green dotted line) was estimated as the number of coactive cells exceeded in a time bin in only 1% of these histograms.

125 Statistical Analysis. Kruskal–Wallis one-way ANOVA combined
126 with multiple-comparison testing was applied to the activities
127 (spikes per minute) of the neurons in all mouse groups to study
128 the statistical similarities. For each mouse category, we used
129 interpolation to account for the different number of neurons
130 recorded in the different animals. Levene’s test was used to

compare the variation within each data group. The variance was
similar between the groups that were statistically compared. A
one-way ANOVA test was used to compare the populations with
USFs, the cells that exhibit USFs, the mean synchronously firing
populations, the mean coactive cells in synchrony peaks, and the
number of synchrony peaks.

PNAS proof
Embargoed

131 187
132 188
133 189
134 190
135 191
136 192
137 193
138 194
139 195
140 196
141 197
142 198
143 199
144 200
145 201
146 202
147 203
148 204
149 205
150 206
151 207
152 208
153 209
154 210
155 211
156 212
157 213
158 214
159 215
160 216
161 217
162 218
163 219
164 220
165 221
166 222
167 223
168 224
169 225
170 226
171 227
172 228
173 229
174 230
175 231
176 232
177 233
178 234
179 235
180 236
181 237
182 238
183 239
184 240
185 241
186 242

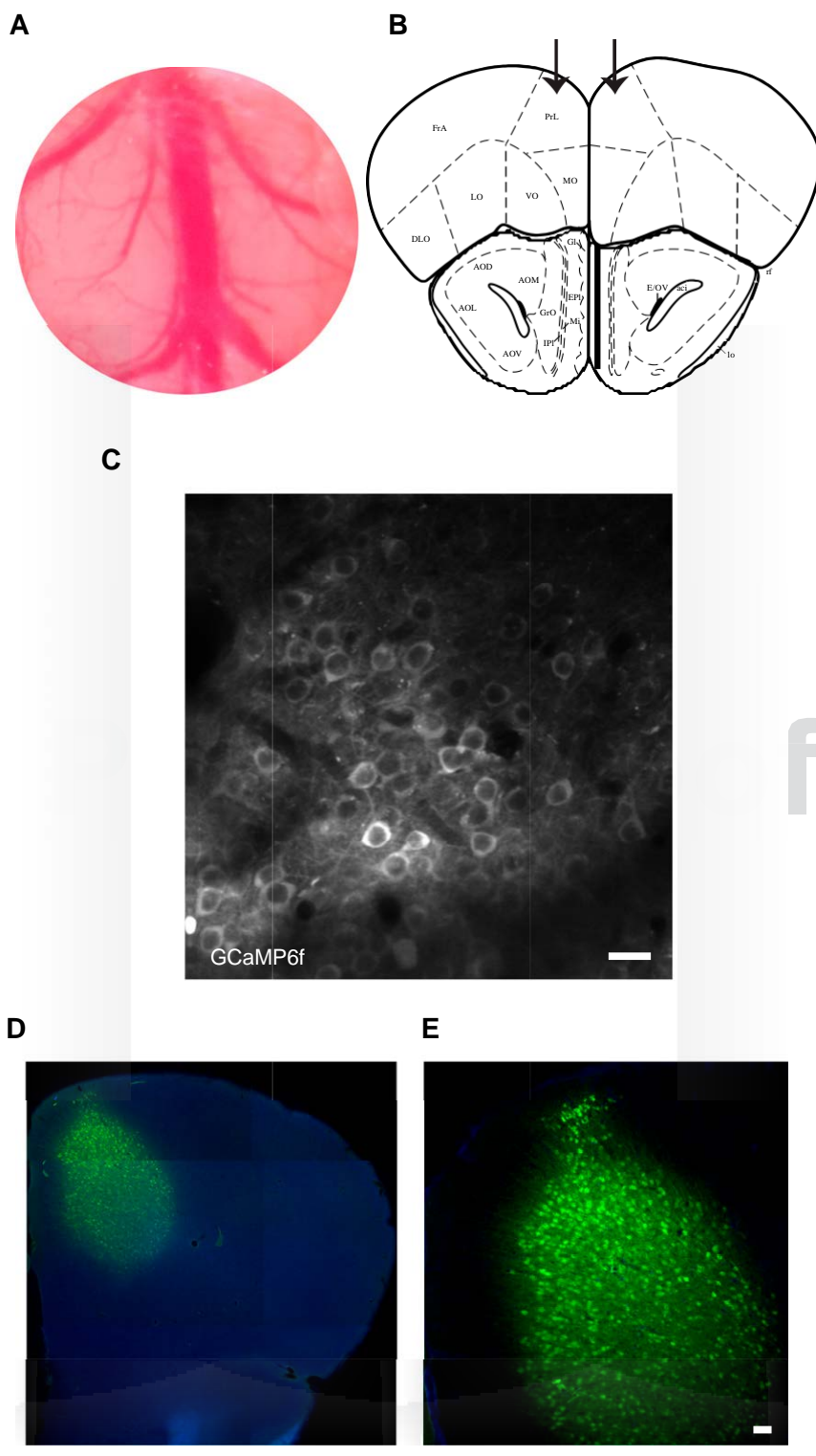


Fig. S1. Two-photon imaging technique and labeling of PFC neurons with GCaMP6f. (A) Photograph of chronic cranial window (5-mm diameter). (B) Coordinates used for the injection of the GCaMP6f: AP, + 2.8 mm from bregma; L, \pm 0.5 mm; and DV, -0.5 to -0.1 mm from the skull surface. The arrows indicate the injection in the PrLC. The scheme was adapted by "The Mouse Brain" from G. Paxinos and K. B. J. Franklin (7). (C) In vivo two-photon image of GCaMP6f labeled neurons in layer II/III of PFC. (Scale bar, 50 μ m.) (D) Mosaic of a 40- μ m coronal section from a WT mouse with GCaMP6f expression (green) and DAPI (blue). (E) Magnification of the cells in C. (Scale bar, 50 μ m.)

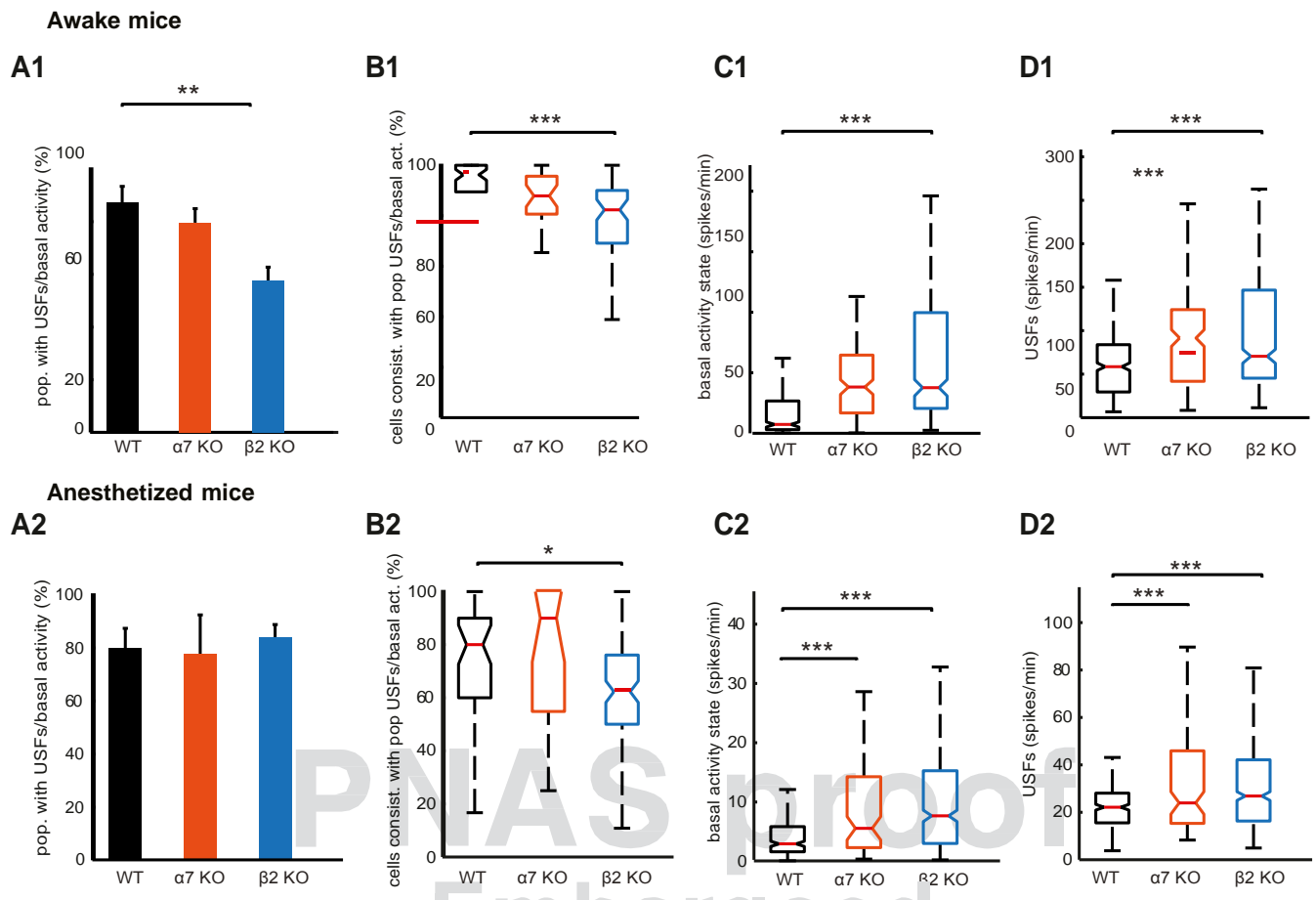


Fig. S2. Properties of USFs transitions in awake and anesthetized mice. (A) Computed percentage of populations that exhibit USFs for each animal type in the awake (A1) and anesthetized state (A2). $\beta 2$ KO mice have a significantly lower proportion of populations that exhibit USFs compared with WT animals. (B) Percentage of cells consistent with populations that exhibit USFs for each animal type in the awake (B1) and anesthetized states (B2). In $\beta 2$ and $\alpha 7$ KO animals, less cells are consistent with populations that exhibit USFs compared with WT mice in the awake state, whereas in the anesthetized state only $\beta 2$ KO are significantly different from WT mice ($P = 0.005$). (C) Boxplots of basal activity states for each mouse type (spikes per minute) in the awake (C1) and anesthetized states (C2). $\beta 2$ and $\alpha 7$ KO animals exhibit significantly higher basal activity compared with WT mice for both the awake and anesthetized state. (D) Boxplots of USFs for each mouse type (spikes per minute) in the awake (D1) and anesthetized states (D2). $\beta 2$ and $\alpha 7$ KO animals exhibit significantly higher USFs compared with WT mice for both awake and anesthetized state. (A1–D1) Awake and (A2–D2) anesthetized mice. * $P < 0.05$, ** $P < 0.01$, and *** $P < 0.001$; ANOVA in A; Kruskal–Wallis in B–D.

497
498
499
500
501
502
503
504
505
506
507
508
509
510
511
512
513
514
515
516
517
518
519
520
521
522
523
524
525
526
527
528
529
530
531
532
533
534
535
536
537
538
539
540
541
542
543
544
545
546
547
548
549
550
551
552
553
554
555
556
557
558

559
560
561
562
563
564
565
566
567
568
569
570
571
572
573
574
575
576
577
578
579
580
581
582
583
584
585
586
587
588
589
590
591
592
593
594
595
596
597
598
599
600
601
602
603
604
605
606
607
608
609
610
611
612
613
614
615
616
617
618
619
620

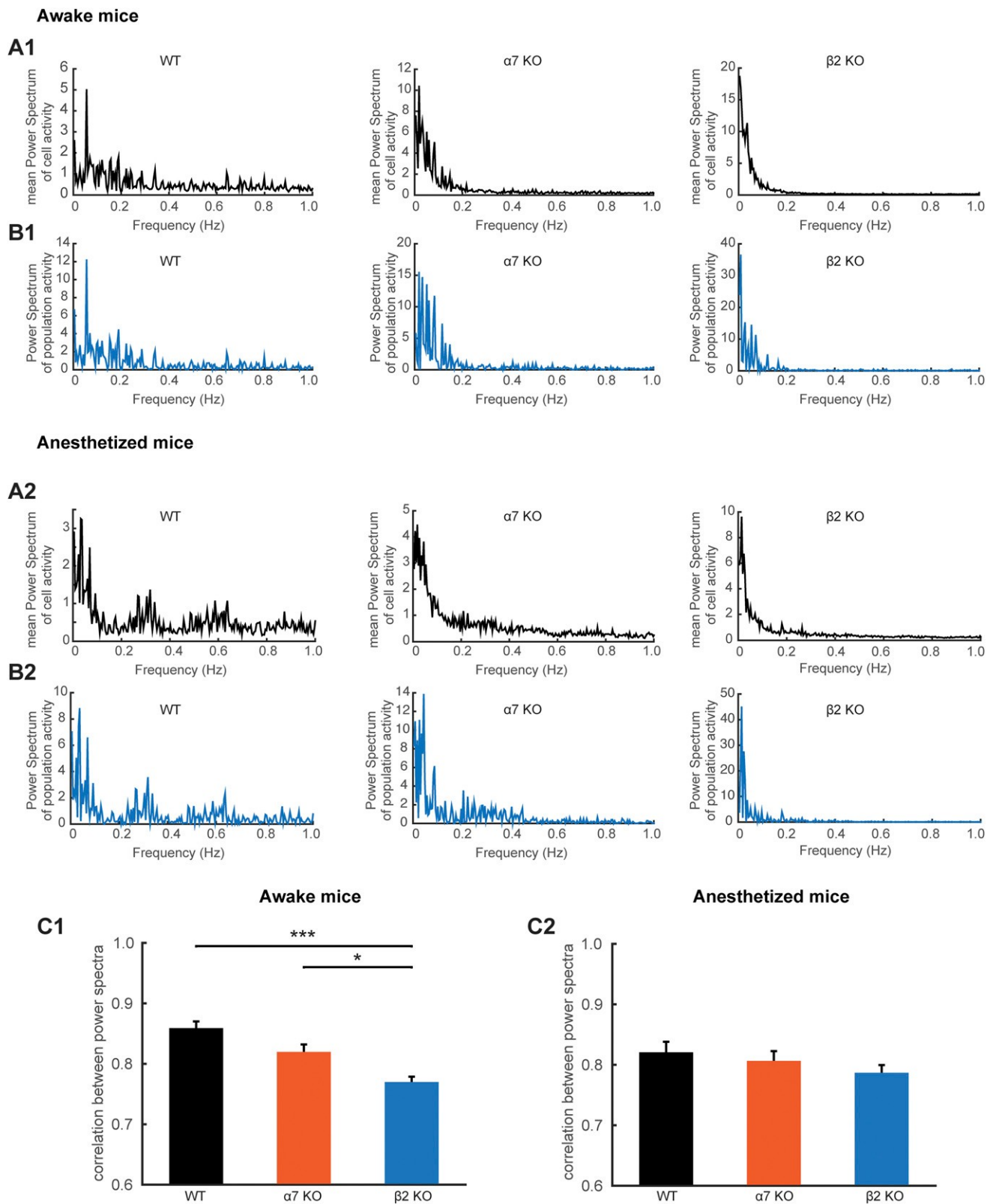


Fig. S3. Power spectrum analysis for the different mouse types in awake and anesthetized state. (A) Comparison of the mean power spectrum of the simultaneously recorded cell activity for WT, $\alpha 7$ KO, and $\beta 2$ KO mice. The power spectrum analysis corresponds to the representative examples described in the main manuscript. (B) Comparison of the power spectrum of the population's activity (mean spiking activity between simultaneously recorded cells). (C) Mean correlation between the mean power spectrum between simultaneously recorded cell activity and the power spectra of the population's activity for the different mouse types. Awake: WT; 0.85 ± 0.014 , $\alpha 7$ KO; 0.82 ± 0.015 , $\beta 2$ KO; 0.78 ± 0.01 . Anesthetized: WT; 0.85 ± 0.021 , $\alpha 7$ KO; 0.79 ± 0.02 , $\beta 2$ KO; 0.80 ± 0.016 . (A1 and B1) Awake and (A2 and B2) anesthetized mice. * $P < 0.05$, ** $P < 0.01$, and *** $P < 0.001$.

621
622
623
624
625
626
627
628
629
630
631
632
633
634
635
636
637
638
639
640
641
642
643
644
645
646
647
648
649
650
651
652
653
654
655
656
657
658
659
660
661
662
663
664
665
666
667
668
669
670
671
672
673
674
675
676
677
678
679
680
681
682

683
684
685
686
687
688
689
690
691
692
693
694
695
696
697
698
699
700
701
702
703
704
705
706
707
708
709
710
711
712
713
714
715
716
717
718
719
720
721
722
723
724
725
726
727
728
729
730
731
732
733
734
735
736
737
738
739
740
741
742
743
744

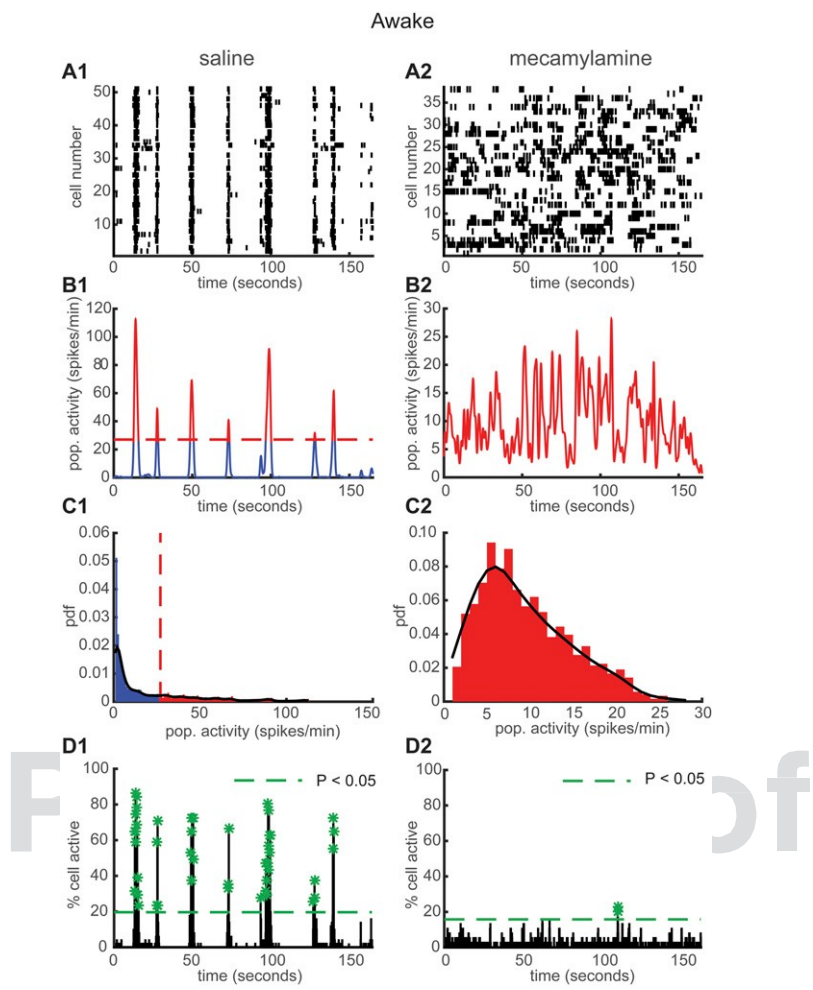


Fig. S4. Chronic exposure to mecamlamine resembles $\beta 2$ KO phenotype. (A) Representative rasterplots for one population of simultaneously recorded neurons in awake WT mice under saline (A1) or mecamlamine (A2) infusion at 7 d after implantation of minipumps. (B) Mean neural activity for the populations in A in WT awake mice under saline (B1) or mecamlamine (B2). Red and blue correspond to USFs and basal activity states, respectively. Dotted red line: computed threshold. (C) Probability density function (pdf) of the population activity exhibited in B in WT awake mice under saline (C1) or mecamlamine (C2). (D) Histogram representing the percentage of cells active in small time bins (~ 0.144 s) for the population activity in A in WT awake mice under saline (D1) or mecamlamine (D2). Asterisks: significant peaks of synchrony.

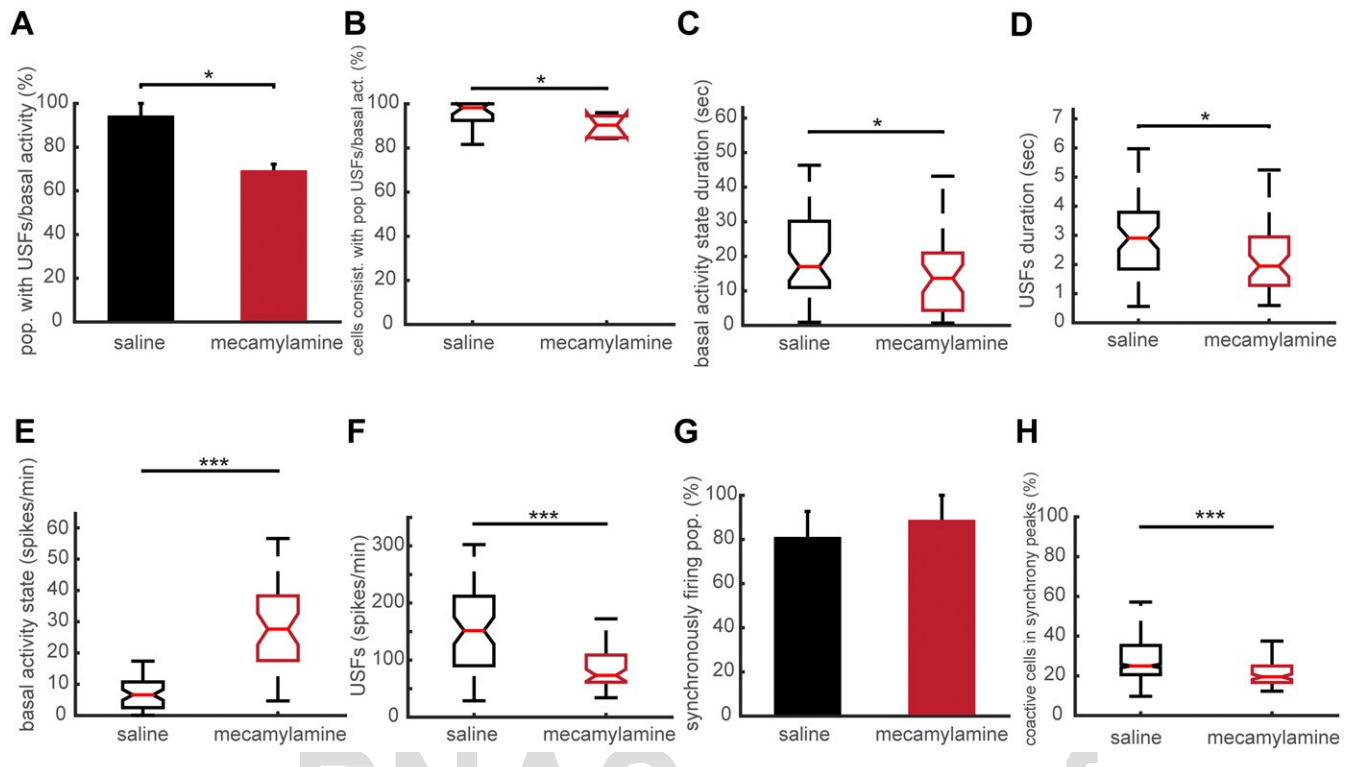


Fig. S5. Properties of USFs transitions in awake WT mice under saline or mecamlamine infusion for 7 d. (A) Computed percentage of populations that exhibit USFs for awake WT mice under saline or mecamlamine infusion at 7 d post implantation of minipump. WT mice under mecamlamine have a significantly lower proportion of populations that exhibit USFs compared with WT mice under saline. (B) Percentage of cells consistent with populations that exhibit USFs for awake WT mice under saline or mecamlamine infusion. In WT animals under mecamlamine less cells are consistent with populations that exhibit USFs compared with WT mice under saline ($P = 0.005$). (C) Boxplots of basal activity durations for each condition in the awake state. WT mice under mecamlamine have a significantly lower basal activity state duration compared with WT under saline. (D) Boxplots of USFs durations for each condition in the awake state. WT mice under mecamlamine have significantly lower USFs duration compared with WT under saline. (E) Boxplots of basal activity states (spikes/min) in the awake state. WT mice under mecamlamine exhibit significantly higher basal activity compared with WT mice under saline. (F) Boxplots of USFs for each condition (spikes per minute) in the awake state. WT mice under mecamlamine exhibit significantly lower USFs activity compared with WT mice under saline. (G) Percentage of populations (simultaneously imaged neurons) exhibiting synchronous activity, for each condition in the awake state. No significant difference between WT mice under saline of mecamlamine infusion. (H) Percentage of coactive cells in the peaks of synchrony for the two conditions in the awake state. * $P < 0.05$, ** $P < 0.01$, and *** $P < 0.001$; ANOV A in A, G, and H; Kruskal–Wallis in B–F.

AUTHOR QUERIES

AUTHOR PLEASE ANSWER ALL QUERIES

Q: 1_Throughout, for concentrations >1%, please state basis (eg, vol/vol, wt/vol, etc).

Q: 2_Please provide a reference for “Image Stabilizer (K. Li).”

Q: 3_Please verify that ref. 7 is the intended reference for the Mouse Brain described in Fig. S1. Ref. 7 is Koch et al, 2016. If this is in error, please add it as new ref. 52, providing all bibliographic information in the reference list.

Q: 4_Please check the locants in Fig. S4 as amended. Locants “B-E” have been changed to “A-D,” respectively.
